Numerical Investigations of Dynamic Stall Phenomenon for Vertical Axis Wind Turbine

Florin Frunzulică * **, *Horia Dumitrescu*** and *Alexandru Dumitrache***
POLITEHNICA University of Bucharest, Faculty of Aerospace Engineering, Polizu 1-6, RO-011061, Bucharest, Romania, e-mail : ffrunzi@yahoo.com
**"Gheorghe Mihoc – Caius Iacob" Institute of Mathematical Statistics and Applied Mathematics, P.O. Box 1-24,RO-010145, Bucharest, Romania*

Abstract
For the vertical axis wind turbines (VAWTs) in urban area, at low tip speed ratio (TSR<4), the dynamic stall is an inherent aerodynamic phenomenon that has a great impact on the structural vibration, noise and power performances. For this reason, in the present work we perform a computational investigation of a two-dimensional dynamic stall phenomenon around a NACA0012 airfoil in oscillating motion at relative low Reynolds number ($\sim 10^5$). The unsteady flow is investigated numerically using RANS approach with two turbulence models ($k-\omega$ *SST* and *transition SST*). The same analysis was performed using three flow control methods (two passive and one active) integrated on/in airfoil.

1. Introduction

In the last years, for home user, the wind turbine with vertical axis (VAWT) began to be more attractive due benefits in exploitation, the power range covering usually the domain 2 kW-20 kW. VAWTs have many advantages over the widely used conventional Horizontal Axis Wind Turbines (HAWTs): operates with wind for any direction (vertical axis => simplify the wind turbine system), designed for low wind speed, operates at low/medium RPM, lower vibration levels, small noise level (quieter in operation due to lower blade-tip speeds) and have lower manufacturing and maintenance cost [1].
But, VAWTs suffer from many complicated aerodynamically problems, of which dynamic stall is an inherent phenomenon when they are operating at low values of tip speed ratio (TSR < 4), and this has a significant impact on vibration, noise, and power output of the VAWTs. In terms of aerodynamics, when the wind speed approaches the speed of operation (for low value of tip speed ratio) the blade airfoil of VAWT exceeds the critical angle of incidence for static conditions. Angle of incidence varies quickly across blade and the blade works in dynamic stall condition. The dynamic stall has an effect of increasing the lift when the incidence increases rapidly and decrease lift when incidence decreases rapidly, compared with aerodynamic static characteristics (delays both flow separation and flow reattachment). These sudden variations of unsteady aerodynamic forces greatly enhance the unsteady loads on the blade and can be dangerous for the structural integrity of the blade [2].
The complexity of the unsteady aerodynamics of the VAWT makes it attractive to be analyzed using Computational Fluid Dynamics, where an approximation of the unsteady Navier-Stokes equations is solved. Based on the Reynolds number, the solver will be set adequately to laminar, transitional or turbulent flow.
In the present study we investigate the following problems: the adequate selection of turbulence model for dynamic stall analysis of isolated oscillating airfoil at Re$\sim 10^5$, and possibility to control dynamic stall.

2. Physics of dynamic stall phenomenon

Previous researches performed by McCroskey et al. [3,4] for airfoil flows, Ferreira et al. [5], Leishman [6], Wernert et al. [7], Lee and Gerontakos [8], revealed complex mechanisms of dynamic stall. Three types of stall can be encountered in aerodynamics: stall onset, light stall and deep stall.
At stall onset the airfoil angle of attack is slightly above the critical angle of attack and small separation begins on the upper side of the airfoil. At this stage increased lift is present without the penalties of increased drag or increased moment. There is a slight hysteresis in the lift coefficient vs. angle of attack diagram.

Light stall occurs as a slightly higher max angle of attack is attained (figure 1.a). A separation bubble is present and turbulent flow is prevalent after the bubble along with a thickening boundary layer. Trailing edge flow reversal is established and the viscous boundary layer thickness at the trailing edge flow separation is about the thickness of the airfoil. The behaviour of light stall is the most sensitive to the effects of airfoil shape, reduced frequency, and Reynolds number. These factors can influence the dominance of trailing edge or leading edge separation.
Deep stall occurs as the angle of attack greatly exceeds the static critical angle of attack (figure 1.b). The deep stall is characterized by the creation of a strong vortex at the leading edge. The vortex is subsequently shed from the boundary layer and moves downstream over the upper surface of the airfoil. As the vortex moves over the airfoil upper surface, values of C_l , C_d and C_m are dramatically increased over their static values. The viscous layer is now about the thickness of one chord length of the airfoil. When the vortex leaves the trailing edge, a large increase in pitching moment known as moment stall and a sharp drop in lift take place. A large amount of hysteresis occurs during this part of the cycle.

a.

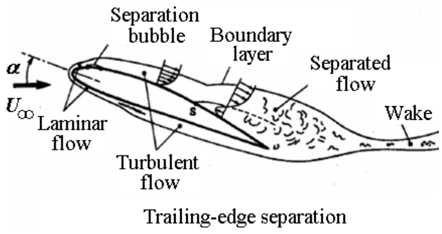

b.

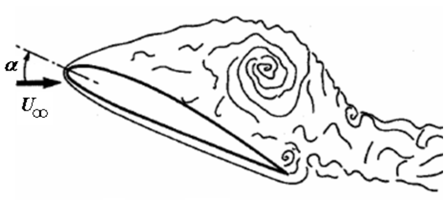

Figure 1: Flow structure - light stall (a) and deep stall (b)

3. Numerical simulations

3.1 Case studied

We investigated numerically the case of the NACA0012 airfoil with a chord length c =15 cm, which executes a sinusoidal pitching motion $\alpha(t)=10^0+15^0\sin(18.67t)$ around point located at ¼ c from the leading edge (corresponding to a reduced frequency $k=\omega c/2V_\infty=0.1$). The airfoil is placed in a free uniform flow with velocity $V_\infty=14\ m/s$ and turbulence intensity of about 1%, which corresponds to a Reynolds number $\mathrm{Re}=1.35\mathrm{x}10^5$. This case is based on the experimental investigations of the dynamic stall phenomenon described in ref. [8].

3.2 Numerical technique

The computational domain is composed by an inner circular domain which executes a rigid pitching motion around its center with angular velocity $\dot{\alpha}(t)=15^0\cdot 18.67\cdot\cos(18.67t)\cdot\pi/180$, and a fixed exterior circular domain with radius 20 c. The hybrid mesh has 760000 nodes; about 1000 nodes are placed on the airfoil surface and clustered close to leading and trailing edges. The height of the first row of cells bounding the airfoil is set to $10^{-5}c$ which ensures $y^+\leq 1$ for a properly resolved of viscous laminar sublayer. The height of the cells expands with a growth factor 1.1 towards to the boundary of the airfoil geometric layer.
For the present study, unsteady Reynolds averaged Navier-Stokes (RANS) model is the suitable approach to perform the dynamic stall flow simulations with an acceptable computational cost and, at least, reasonable accuracy. We used Ansys Fluent code for computational simulations [9]. Due to the incompressibility of the investigated flow, the unsteady pressure-based solver is chosen. All the governing equations for the solution variables, which are decoupled from each other, are solved sequentially and the SIMPLEC algorithm is applied as the pressure-velocity coupling algorithm. With respect to the discretization of the convection terms in the transport equations for the velocity and the turbulence quantities, second-order upwind schemes are utilised. In order to accelerate the rate of convergence of the solution, the algebraic multigrid scheme with a W-cycle type for the pressure and the momentum equations is applied.
The numerical time step is set to be 0.1 ms based on the characteristic time flow; after two complete oscillations the solution became periodical.

3.3 Turbulence models

Two turbulence models are used in the present work: $k-\omega\ SST$ (Shear Stress-Transport Turbulence Model) proposed by Menter [10] and *transition SST* proposed by Langtry & Menter [11].
1. *Turbulence model:* $k-\omega\ SST$. The basic idea behind the SST model is to retain the robust and accurate formulation of the Wilcox $k-\omega$ model in the near wall region, and to take advantage of the free stream independence of the $k-\varepsilon$ model in the outer part of the boundary layer. In order to achieve this aim, the $k-\varepsilon$ model is transformed into a $k-\omega$ formulation by means a function F_1 that is one in the near wall region and zero away from the surface [10].
2. *Transition SST model.* The transition SST model is based on four transport equations [11]. One transport equation is for intermittency (γ), which can be used to trigger transition locally. The intermittency function is coupled with the two transport equations of the $k-\omega\ SST$ turbulence model. It is used to turn on the production term of the turbulent kinetic energy downstream of the transition point based on the relation between transition momentum-thickness and strain-rate Reynolds number.
A fourth transport equation is applied for the transition onset momentum-thickness Reynolds number (Re_θ). This is required in order to capture the non-local influence of the turbulence intensity, which changes due to the decay of the turbulence kinetic energy in the free-stream, as well as due to changes in the free-stream velocity outside the boundary layer. This transport equation is an essential part of the model as it ties the empirical correlation to the onset criteria in the intermittency equation.

3.4 Results

Figure 3 presents streamlines and static pressure contours at different angles of attack during the dynamic stall process (after the solution became periodic). In upstroke phase we can observe the following:
- for range $-5^0 \le \alpha \le 11^0$ the flow is fully attached to the airfoil;
- at about 11.5^0 a thin laminar separation bubble appears close to the leading edge; after this bubble the boundary layer is turbulent (with $k-\omega\ SST$ the bubble appears at approx. 19^0) (figure 4);
- the laminar bubble grows in size and travels towards the trailing edge; at about 18.4^0 it has a length of 1/3 c on the upper surface and it has completely turned into leading edge vortex;
- at about 24.1^0 the leading edge vortex covers the whole upper surface of the airfoil; at this moment the C_l reaches the maximum value;
- at 24.35^0, the leading edge vortex begins detaching from the airfoil surface; it carries a pair of vortices at the leading edge;
- at 24.7^0, the trailing edge vortex has grown and the leading edge vortex becomes weak in intensity;
- at maximum angle of attack, the flow structure on the upper side contains a pair of vortices at leading edge and a trailing edge vortex;
- the thin layer of reversed flow near the suction side is significantly unstable and easily breaks down into several small-scale vortices in upstroke phase;
- the used turbulence models give a good agreement with the experimental data, but the transition SST model perform best the maximum lift coefficient. Figure 5 shows a comparison between our numerical simulations and results published in ref [8, 12].

In the downstroke phase flow is more complex with the following characteristics:
- the trailing edge vortex grows in size and at about 23^0 sheds in the wake;
- at about 22^0 the pair of vortices cover the whole upper surface;
- at 21.5^0 the second vortex sheds in the wake; the last vortex generated on the suction surface grows in size and sheds at 10^0;
- under 10^0 the flow begins to reattach on the upper surface;
- the turbulence models falls in prediction of flow characteristics; the transition SST model gives, with a reasonable accuracy, a better evaluation of the flow characteristics than $k-\omega\ SST$ model.

Under the operating conditions in this case, a large difference of the solutions compared to the experimental data during the downstroke pitching phases is observed. The turbulence models haven't ability to reproduce exact the experiment in the downstroke phase; it is necessary more investigation of turbulence models.
The oscillations in the lift coefficients at small incidence, where the flow is assumed to be non-separated, imply that the $k-\omega\ SST$ turbulence model is very sensitive in the present unsteady low turbulence intensity flow application.

The computational results qualitatively capture well the features of the dynamic stall process, such as the formation, convection and shedding of the leading edge vortex as well as the secondary vortex, and these predictions provide information on the flow development.

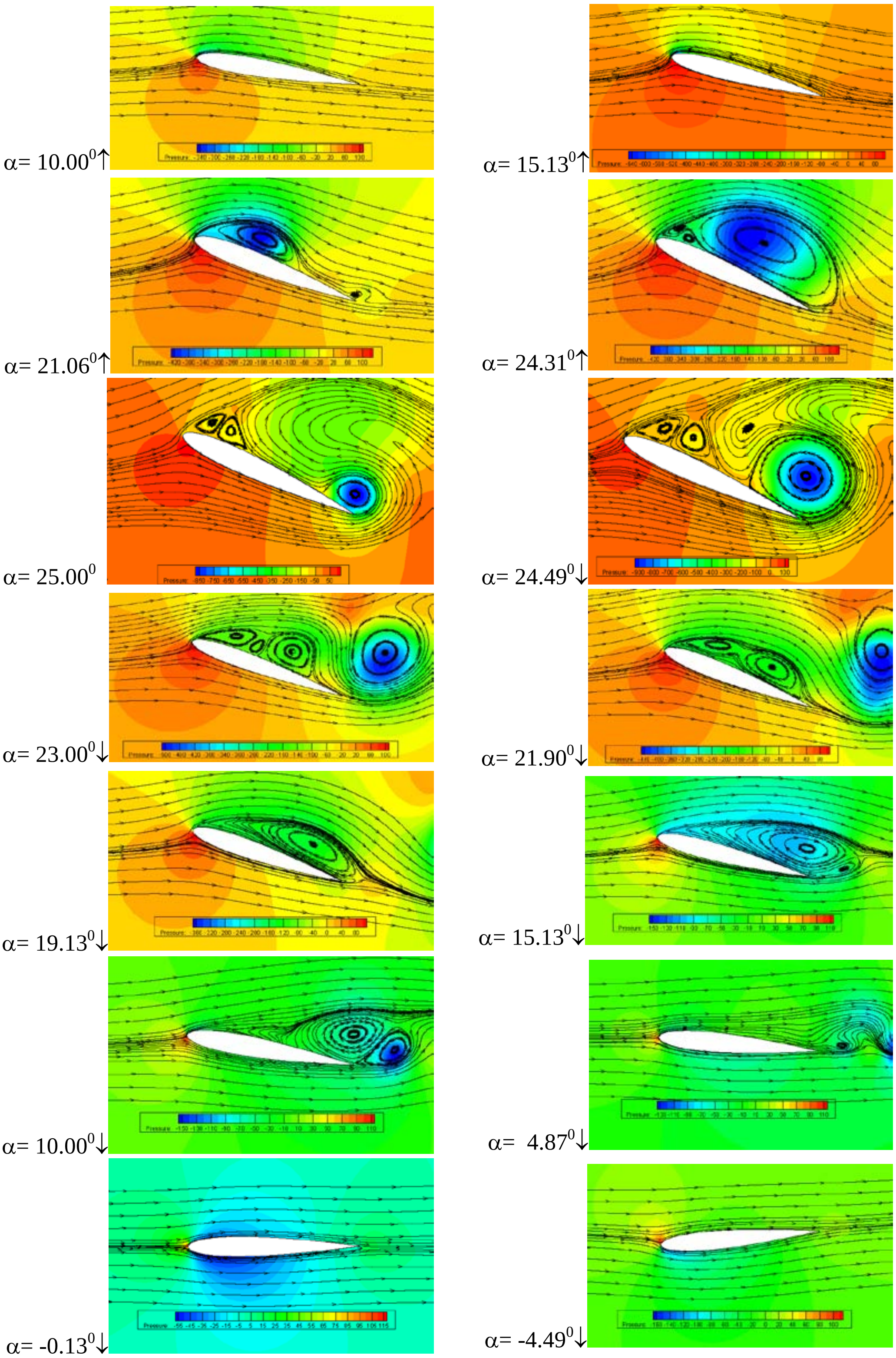

Figure 3: Streamlines and static pressure contours ($\Delta p = p - p_{ref}$) at different angles of attack during the dynamic stall process, using transition SST model.

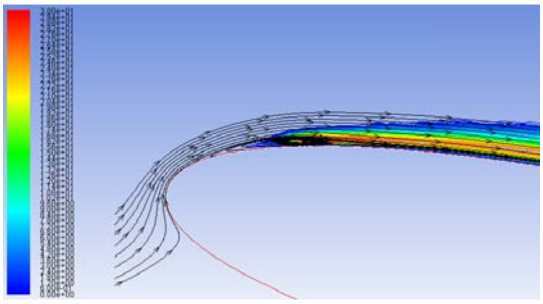

Figure 4: Turbulent viscosity ratio after laminar separation bubble

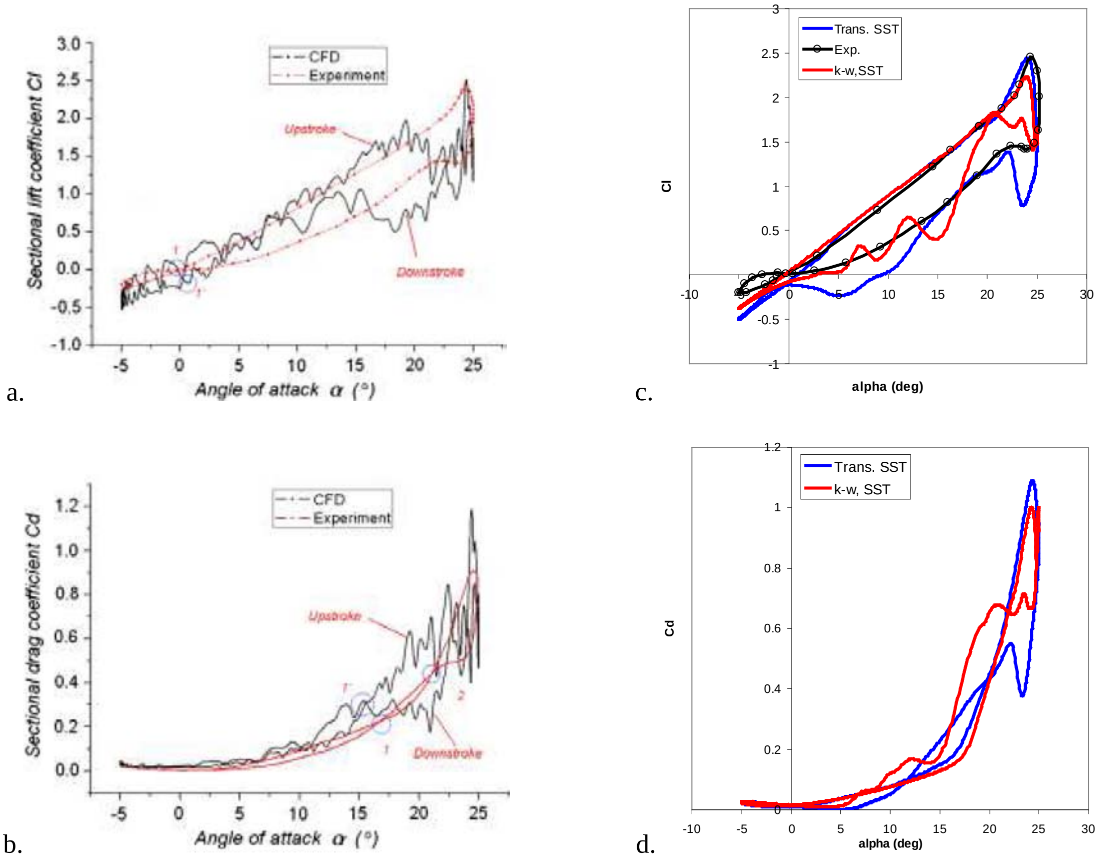

Figure 5: Aerodynamic coefficients – C_l and C_d : a. and b. from ref. [12] ; c. and d. from present numerical simulation.

For the next computational cases we used the transition SST turbulence model.

4. Dynamic stall control

4.1 Passive control. Gurney flap

A technique to enhance the lift of airfoils is to use passive devices, one of these being known as Gurney flap. The Gurney flap, first introduced by Liebeck [13], is a small tab attached perpendicular to the lower surface of the airfoil in the vicinity of the trailing edge, with a height that can vary from 1% to 5%. The results showed a significant increment in lift compared to the baseline airfoil. This device increases the drag, but the percentage increase in lift is greater, resulting in an increased lift/drag ratio and therefore a better efficiency and performance. The flow structure downstream of a Gurney flap has a dual recirculation region that produces increasing lift due the significant turning of the upper-surface trailing-edge flow (figure 6.a) and reduces form drag due the longer region of attached flow near the trailing edge.

A systematic studies [14] concluded that a Gurney flap with a typically height 1%-2% *c* works well, with a lowest drag increase. However, due to large range of angle of attack during dynamic stall process, on the lower surface of the airfoil the trailing-edge boundary layer thickness changes by a large amount, making the flap height un-satisfactory. Increasing height flap increases the local stagnation region, deflecting the free stream flow away from the lower surface and increasing of flow separation from the flap and also causes the trailing edge stagnation point to move progressively downstream into wake [15].
Due to its simple geometry, construction of the Gurney flap is simple and implementation of this device is easily accomplished. Gurney flap has used in many applications, e.g., alleviation of airfoil static and dynamic stall, flutter control, and rotor blade control.

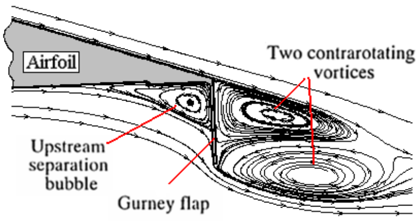

a.

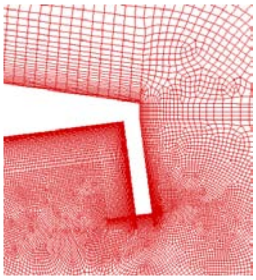
b.

Figure 6: Gurney flap: flow around flap (a) and detail of mesh (b).

Numerical simulation. The mesh is build on the same principles as the mesh for unchanged airfoil; at trailing edge we put a Gurney flap perpendicular to the lower surface of the airfoil, with $h/c = 1$ % and thickness $\delta = h/5$ (figure 6.b).
The figure 7 shows the contour of the pressure field ($\Delta p = p - p_{ref}$) superimposed to the instantaneous streamlines computed with the transition SST model. The flow in time is almost similar to flow on the original airfoil, but vortical structure generated at leading edge remain long time attached to a upper-side of the airfoil increasing lift especially in upstroke motion. After angle of attack about 24.10^0 in upstroke the vortex diffuses in wake and appears a sudden decrease of lift. In downstroke motion, after maximum angle of attack (25^0), the vortex generated at trailing edge increases and at leading edge appears a structure of vortices. At about 23.40^0 the trailing edge vortex pass in the wake and on the upper surface vortices generated at leading edge will create a vortical structure which increases the lift in the downstroke stage. After vortex exceeds the trailing edge of the airfoil and it is moved in downstream turbulent wake, the flow on the upper-side of the airfoil evolves to a complete separation state and we have a loss of lift. When the angle of incidence is small enough (less than 10^0), the flow is reattached again beginning from the leading edge.

$\alpha = 4.87^0\uparrow$ 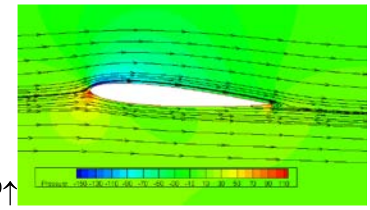

$\alpha = 10.00^0\uparrow$ 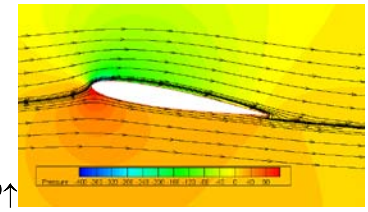

$\alpha = 15.13^0\uparrow$ 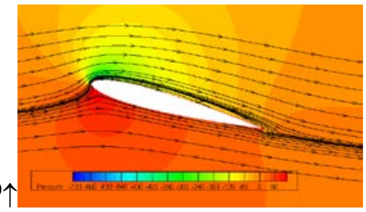

$\alpha = 20.13^0\uparrow$ 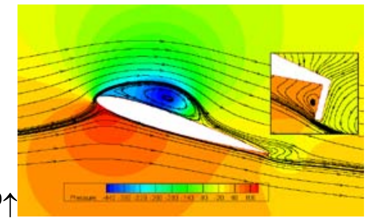

$\alpha = 24.10^0\uparrow$ 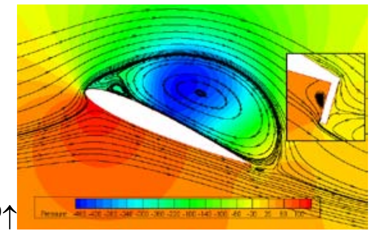

$\alpha = 25.00^0$ 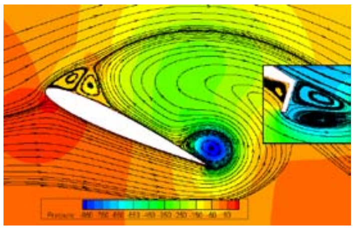

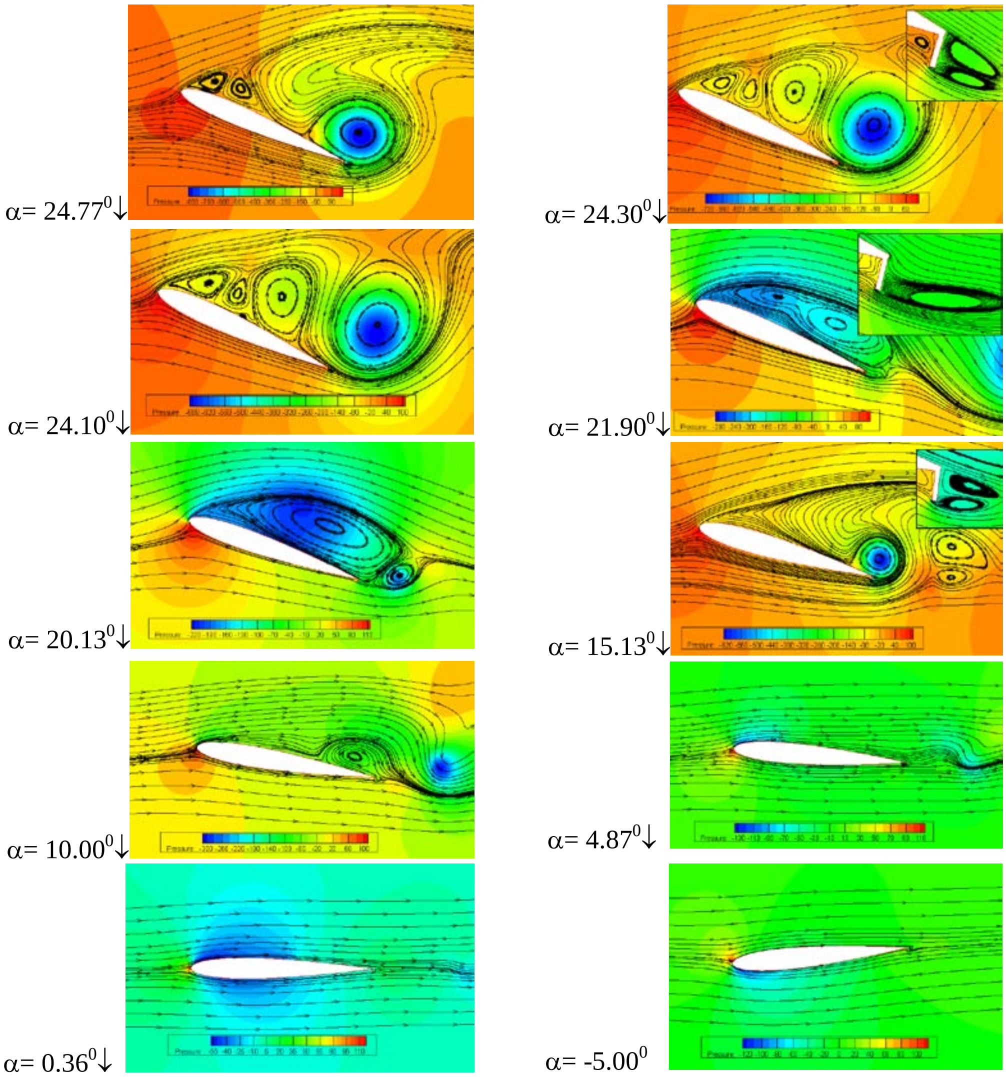

Figure 7: Gurney flap - streamlines and static pressure contours ($\Delta p = p - p_{ref}$) at different angles of attack during the dynamic stall process, using transition SST turbulence model.

4.2 Passive control. Thin channel

Another passive device uses a slot between lower-pressure and high-pressure points (near the separation point) on the upper surface of the airfoil (at positive angle of attack). The tendency of redistribution of the pressure will maintain the boundary layer attached to the upper surface. Thus the form drag is reducing and the lift changes the orientation. Mounting on the channel a controlled hydraulic resistance we can control the separation point of the boundary layer. The advantage of this method is that not implying additional source of power and can be used as a passive/active control of flow.
The settings are the same as the previously cases. Figure 8 shows a detail of a thin channel; the channel, with 1 mm thickness, unites points placed at 15% *c* and 75% *c* from the leading edge, on the upper surface of the airfoil.

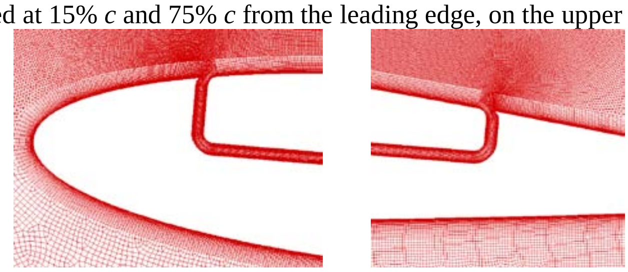

Figure 8: Details of mesh.

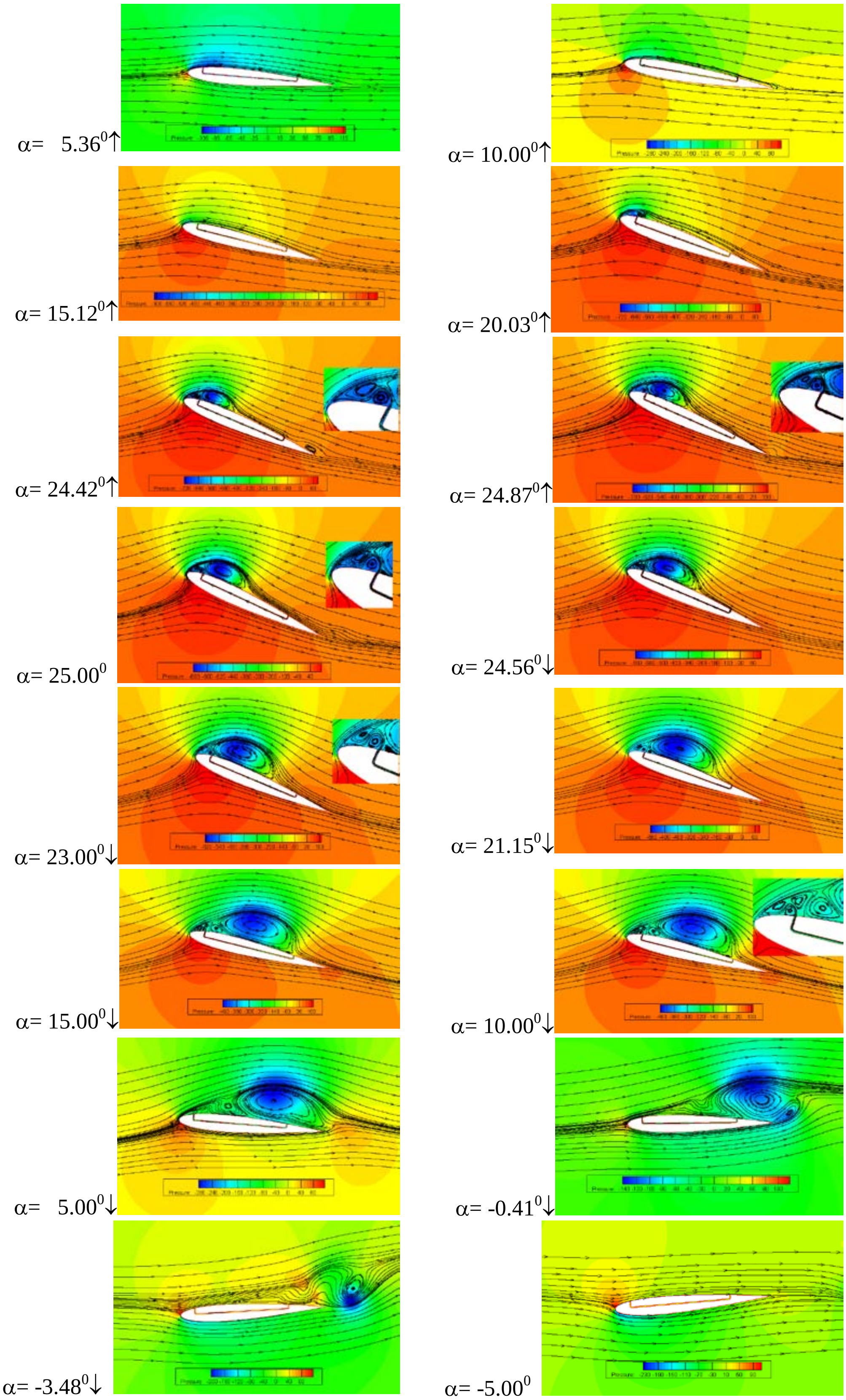

Figure 9: Thin channel - streamlines and static pressure contours using transition SST turbulence model.

During the dynamic stall, at positive angle of attack, appears in channel a laminar secondary flow between the second point, where exits high pressure (suction), and the first point where is lower pressure (blowing). As a result the flow remains attached to the upper surface until about 19^0 in upstroke regime. After this value appears at leading edge a vortex which deviates forward the flow blowing through the first orifice and creates two vortices near the leading edge. In downstroke phase, surprising the vortex structures growth slowly and lift continues to increase until 21.15^0 (figure 9). The main vortex structure travels toward the leading edge, pass over the second orifice where the vortex intensity grow down. At about 0^0 the vortex leaves the upper surface of the airfoil (downstroke phase).

4.3 Active control. Blowing jet at trailing edge

In this section we analyze active control with jet, with additional flow mass (forced jet). Circulation control is know as beneficial in increasing the bound circulation and hence the lift coefficient of airfoil. This technology has been investigated both experimentally and numerically [15] in the last decade. Circulation control is implemented, usually, by tangential blowing a small high-velocity jet over a highly curved surface, such as a rounded trailing edge. This causes the boundary layer and the jet to remain attached along the curved surface due to the Coanda effect (the tendency of a moving fluid to attach itself to a surface and flow along it) and causing the jet to turn without separation (figure 10).

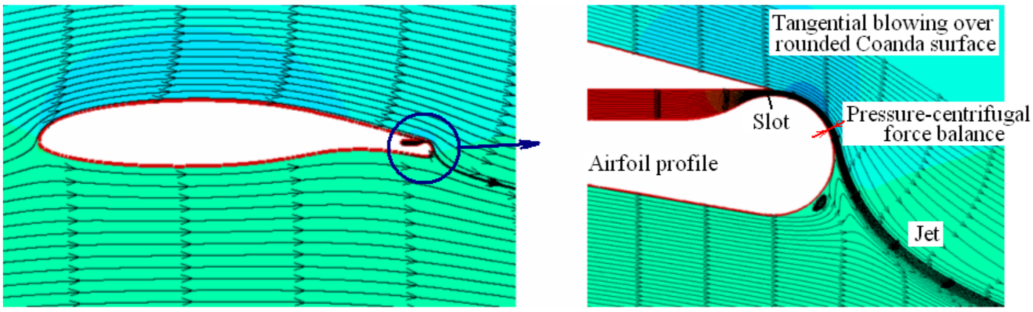

Figure 10: Blowing jet over Coanda surface at trailing edge.

The rear stagnation point moves toward the lower surface, producing additional increase in circulation around the airfoil, leading to high value of lift coefficient comparable to that achievable from conventional high lift devices. The airfoil with this device has a large-radius rounded trailing edge (to maximize the lift), and the drag increase substantially when the jet is turned off. One possible way to reduce this drag is to make the lower surface of the trailing edge as a flat surface. The circulation control for design of wind turbine is advantageous because any increase in the magnitude of the lift force (while keeping drag small, and lift/drag high) will immediately contribute to a increasing in induced thrust and torque. If the flow over the airfoil separates at the leading edge is necessary secondary Coanda jets at the leading edge to maintain the flow attached to airfoil.
Forced jets have a few disadvantages: complexity of internal piping from a source of pressure or vacuum, and the parasitic cost to produce this pressure. While circulation control with forced jets has the potential for increased power generation, the power is consumed in the generation of the jet. A challenge is to reduce the power consumption to produce the jet and using efficiently the jet to control flow separation.
It is recognized that the efficiency of a rectangular slot depends on the geometry of its section (dimensions ratio in the section plane). The efficiency studies for rectangular slots are limited to the aspect ratio of 10 (Aspect Ratio = *w/h*) while for similar studies used in circulation control this ratio is higher than 1300 [16]. Therefore for the two-dimensional study presented, the efficiency of the slot might be neglected and it can be presumed that there are no (pressure) losses. Whereas for the circulation control two-dimensional study the thrust might be assessed at the airfoil exit of the blown jet using the impulse or thrust coefficient:

$$C_\mu = \frac{Thrust}{q\,S} = \frac{\dot{m}V_{jet}}{q\,S} = \frac{2\,h\,w}{b\,c}\frac{\rho_{jet}}{\rho_\infty}\frac{V_{jet}^2}{V_\infty^2} \qquad \textbf{(1)}$$

where

$$\dot{m} = \rho_{jet} V_{jet} h\, w\,, \qquad \textbf{(2)}$$

and *S* is the wing reference surface (considered as rectangular), while

$$V_{jet} = \sqrt{\frac{2\chi R T_{0,\,jet}}{\chi - 1}\left[1 - \left(\frac{p_\infty}{p_{0,\,jet}}\right)^{\frac{\chi-1}{\chi}}\right]} \qquad \textbf{(3)}$$

For a rough estimation of the fluid's power, P_f, it is presumed that the jet is supplied by a big reservoir. Then, the total power will be at least equal with the power required to supply the control device to create the jet (P_{jet}) plus the lost power in the intake device of the big reservoir (P_{rez}):

$$\begin{aligned} P_f &= P_{jet} + P_{rez} \\ &= \frac{1}{2}\rho V_{jet}^2 \frac{\dot{m}}{\rho} + \dot{m} V_\infty^2 \end{aligned} \quad \mathbf{(4)}$$

Also, the necessary power to be supplied for the flow with the impulse coefficient C_μ is:

$$P_f = C_\mu \frac{V_{jet}}{2V_\infty}\left[1 + 2\frac{V_\infty^2}{V_{jet}^2}\right](q_\infty V_\infty S) \quad \mathbf{(5)}$$

or dimensionless

$$C_{P_f} = \frac{P_f}{q_\infty V_\infty S} = C_\mu \frac{V_{jet}}{2V_\infty} + C_\mu \frac{V_\infty}{V_{jet}} \quad \mathbf{(6)}$$

If the slot height *h* is constant and known for a rectangular wing or blade, the fluid power might be expressed as a function of the coeffcient C_μ and the slot height /airfoil chord ratio (*h/c*):

$$C_{P_f} = \frac{C_\mu^{3/2}}{2\sqrt{2(h/c)}}\left[1 + \frac{4(h/c)}{C_\mu}\right] \quad \mathbf{(7)}$$

Figure 11 shows the dependence of the ideal power coeffcient as function of the impulse coefficient.

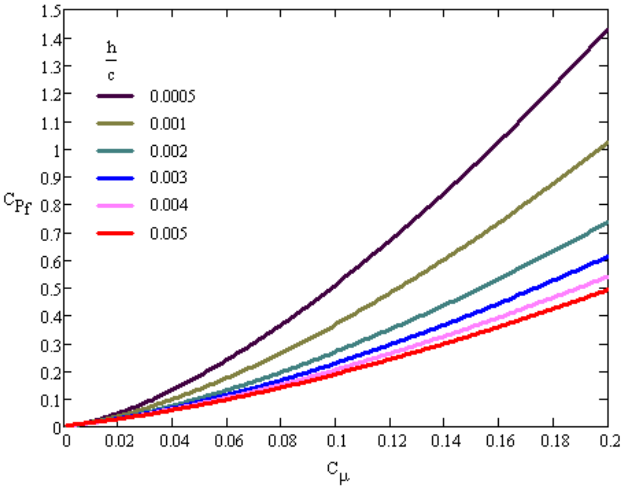

Figure 11: Necessary theoretic power for typical ”Coandă” jets with different *h/c* ratio.

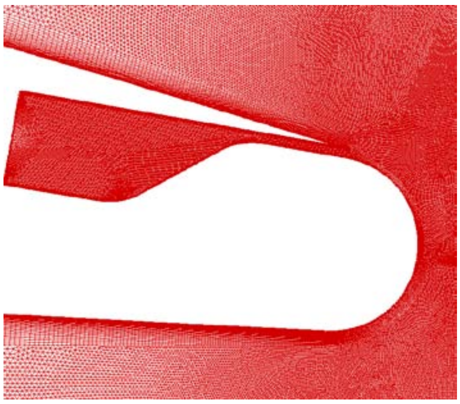

Figure 12: Local mesh of the trailing edge.

Figure 12 shows geometry and local mesh for present configuration. We kept the geometry of the NACA0012 airfoil and at 92 % we create a rounded surface as a trailing edge; the ratio *h/c* is set to about 0.15%. The jet has the impulse coefficient $C_{\mu} = 0.02$ and remains attached a short length on rounded surface (low impulse of jet).

At about 20^0 in upstroke phase appears leading edge vortex which grows in size and lift increases quasi-linear with angle of attack toward the 25^0 (figure 13). A small separation region with reattachment can be observed near trailing edge on the upper surface at about 25^0. In downstroke phase, the leading edge vortex increases and a consequence the lift increase slowly until the angle of attack become 20^0. After this value near leading edge on the upper surface,

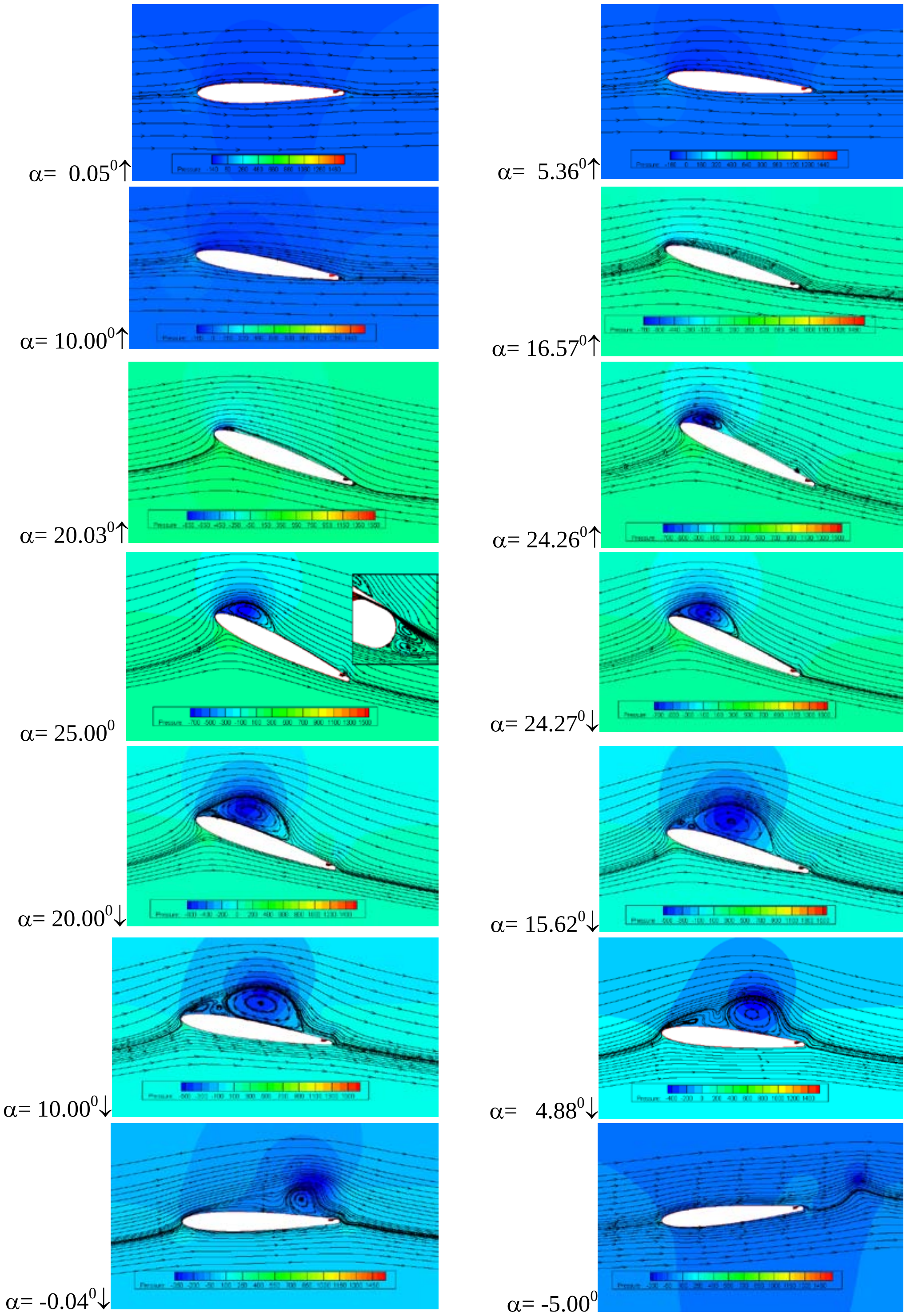

Figure 13: Blowing jet at trailing edge - streamlines and static pressure contours using transition SST turbulence model.

a pair of vortices appears, which increase in size and intensity while the main vortex grow down in intensity and travels to the leading edge. At about 5^0 the pair of vortices diffuses in the exterior flow and at about -3^0 the vortex that exists on the upper surface diffuses in the wake.

4.4 Aerodynamic coefficients

In the figure 14 the aerodynamic coefficients C_l, C_d and C_m are shown. We noted that for current numerical simulations the momentum coefficient is negative when the angle of attack grows (the airfoil is placed in the XOY plane).

In the case of Gurney flap, we can see that the transition SST turbulence model produces a good evaluation of aerodynamic coefficients in upstroke phase, but in downstroke phase presents too sharp a drop-off of the C_l between 25^0 and 10^0 angle of attack. It's clear that the Gurney flap produces more lifting effect than in the basic case and is a good alternative to amplify the dynamic stall. Near maximum angle of attack we observe a sudden variation of C_l and C_d which can produces structural vibration.

The passive control with a thin channel assures (for positive angle of attack) a quasi-linear dependence of a lift coefficient with angle of attack in upstroke phase and in downstroke phase the lift coefficient has a greater value than in upstroke phase. The drag coefficient is small than in the basic case and the pitching moment is greater in the downstroke phase.

The active control with a thin jet assures a positive C_l during dynamic stall process, the small C_d than the basic case and the pitching moment is greater in downstroke phase.

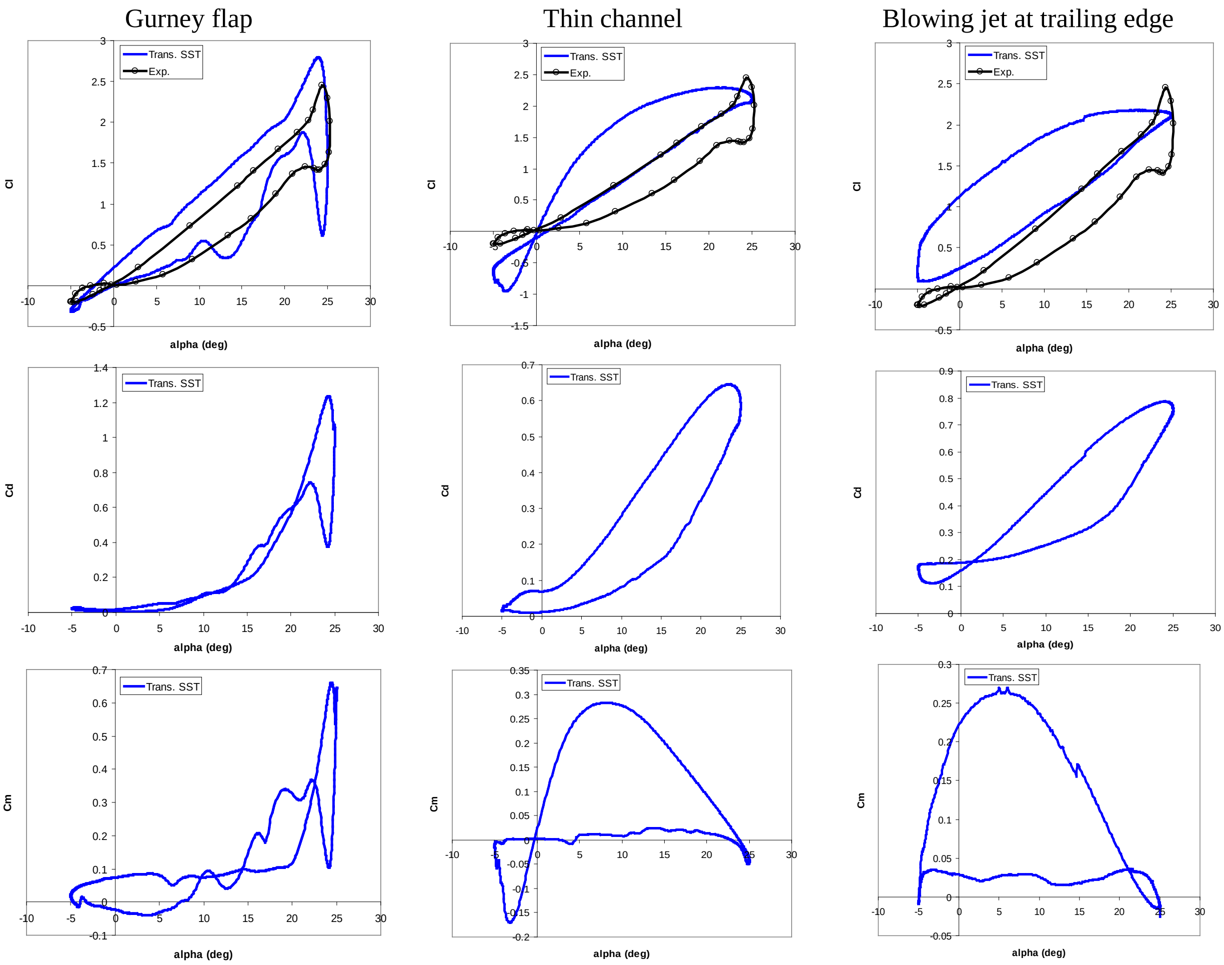

Figure 14: Aerodynamic coefficients for the controlled dynamic stall phenomenon

5. Conclusions

In this paper, two RANS turbulence models, namely the $k-\omega$ *SST* and the transition *SST* model have been used to simulate the fluid flow around a NACA 0012 airfoil executing a sinusoidal pitching, in the low Reynolds number fluid flow regime. The two turbulence models employed can predict the experimental data with good accuracy in upstroke phase, but in downstroke phase the models cannot predict very well experimental data, especially at high angle of attack. Our point of view is that the transition SST model performs best the dynamic stall process at relative low Reynolds.

We investigated three possibilities to enhance the dynamic stall phenomenon: Gurney flap, thin channel and blowing jet at trailing edge, using transition SST model. In our simplified study, all methods have potential to improve phenomenon at low tip speed ratio for VAWTs. Gurney flap works very well in upstroke phase while and the last two assures a increasing of lift coefficient and pitching moment in the downstroke phase. We conclude that the combination of these methods can enhance dynamic stall phenomenon in the starting phase and at low tip speed ratio, increasing performances for VAWTs.

Acknowledgement

This work was realised through the Partnership programme in priority domains - PN II, developed with support from ANCS CNDI - UEFISCDI, project no. PN-II-PT-PCCA-2011-3.2-1670

References

[1] Dumitrescu, H., V. Cardos, and Al. Dumitrache. 2001. Aerodynamics of wind turbines. Romanian Academy Publihing House.
[2] Dumitrescu, H., V. Cardos, F. Frunzulica, and Al. Dumitrache. 2007. Unsteady aerodynamics, aeroelasticity and aeroacoustics for wind turbines. Romanian Academy Publishing House, ISBN 978-973-27-1394-5.
[3] McCroskey, W., L. Carr, and K. McAlister. 1976. Dynamic stall experiments on oscillating airfoils. *AIAA J*. 14: 57–63.
[4] McCroskey, W., K. McAlister, L. Carr, and S. Pucci. 1982. An experimental study of dynamic stall on advanced airfoil sections. Summary of the experiment. Vol. 1. NASA Technical Memorandum 84245.
[5] Ferreira, C., H. Bijl, G. van Bussel, and G. van Kuik. 2007. Simulating dynamic stall in a 2D VAWT: modeling strategy, verification and validation with particle image velocimetry data. *J Phys Conf* Ser;75.
[6] Leishman, J. 1990. Dynamic stall experiments on the NACA 23012 aerofoil. *Exp Fluids*, 9(1):49–58.
[7] Wernert, P., W. Geissler, M. Raffel, and J. Kompenhans. 1996. Experimental and numerical investigations of dynamic stall on a pitching airfoil. *AIAA journal,* 34: 982-989.
[8] Lee, T., and P. Gerontakos. 2004. Investigation of flow over an oscillating airfoil. *J Fluid Mech*, 512:313–41.
[9] Ansys Fluent 12. User's guide. Fluent documentation.
[10] Menter, F. 1994. Two-equation eddy-viscosity turbulence models for engineering applications. *AIAA J*, 32(8):1598–605.
[11] Langtry, R.B., and F. Menter. 2005. Transition modeling for general CFD applications in aeronautics. AIAA Paper 2005-522.
[12] Wang, S., Ingham, D.B., MaLin et al. 2010. Numerical investigation on dynamic stall of low Reynolds number flow around oscillating airfoils. *J Computer & Fluids*, 39: 1529-1541.
[13] Liebeck, R.H. 1978. Design of subsonic airfoils for high lift. *J. Aircr.* 15: 547-561.
[14] Giguere, P., G. Duma, and J. Leway. 1997. Gurney flap scaling for optimum lift-to-drag ratio. *AIAA J.*, 35: 1888-1890.
[15] Meyer, R., W. Hage, et al. 2006. Drag reduction on Gurney flap by three-dimensional modifications. *J. Aircr.* 43: 132-140.
[16] Applications of circulation control technologies. 2006. Progress in Astronautics and Aeronautics. vol. 214. Edited by Ronald D. Joslin and Gregory S. Jones.